Geophysical Research Letters

RESEARCH LETTER
10.1029/2023GL103339

Do Optically Denser Trade-Wind Cumuli Live Longer?

Torsten Seelig[1], **Felix Müller**[1], **and Matthias Tesche**[1]

[1]Leipzig Institute for Meteorology (LIM), Leipzig University, Leipzig, Germany

Key Points:

- First study of the life cycle of shallow marine cumulus based on observations with the Advanced Baseline Imager aboard GOES-16
- Confirmation of the double power law in the distribution of cloud lifetime from measurements with a temporal resolution of 1 minute
- Cloud lifetime is related to large-scale circulation and affects cloud optical thickness

Supporting Information:

Supporting Information may be found in the online version of this article.

Correspondence to:

T. Seelig,
seelig@uni-leipzig.de

Citation:

Seelig, T., Müller, F., & Tesche, M. (2023). Do optically denser trade-wind cumuli live longer? *Geophysical Research Letters*, *50*, e2023GL103339. https://doi.org/10.1029/2023GL103339

Received 17 FEB 2023
Accepted 15 JUN 2023

Author Contributions:

Conceptualization: Torsten Seelig, Matthias Tesche
Formal analysis: Torsten Seelig
Funding acquisition: Matthias Tesche
Investigation: Torsten Seelig
Methodology: Torsten Seelig
Software: Torsten Seelig, Felix Müller
Visualization: Torsten Seelig
Writing – original draft: Torsten Seelig, Felix Müller, Matthias Tesche
Writing – review & editing: Torsten Seelig, Felix Müller, Matthias Tesche

Abstract This study investigates the lifetime and temporal evolution of physical properties of trade-wind cumuli based on tracking individual clouds in observations with the Advanced Baseline Imager aboard the geostationary GOES-16 satellite during the "ElUcidating the RolE of Cloud–Circulation Coupling in ClimAte" (EUREC^{4}A) campaign east of Barbados in winter 2020. A first application of our upgraded cloud-tracking toolbox to measurements with high spatio-temporal resolution (2×2 km^2 and 1 min) provides probability density functions of lifetime and area of clouds that develop as a consequence of meso-to-synoptic scale motions. By separately considering clouds that exist during daytime and live in distinct lifetime intervals, we find that shallow marine cumuli live longer when they cover a larger surface area and show higher cloud optical thickness (COT). Besides the effect of COT, the scale of the atmospheric motions with which the clouds interact is also critical to their lifetime.

Plain Language Summary We present a detailed investigation of the lifetime of Caribbean trade-wind cumulus clouds and the temporal evolution of their physical properties based on geostationary observations with the Advanced Baseline Imager aboard the geostationary GOES-16 satellite during the "ElUcidating the RolE of Cloud–Circulation Coupling in ClimAte" (EUREC^{4}A) field experiment in winter 2020. The tracking of 2.7 million individual clouds in measurements with high spatio-temporal resolution enables the investigation of processes that control the lifetime of shallow marine cumulus (SMC) clouds. Our analysis reveals that SMC clouds live longer when they span over a surface area that exceeds an order of tens of square kilometers. While these clouds show similar median cloud droplet size and number concentration compared to shorter-lived clouds, they contain more liquid water and, thus, show a COT that is increased by about one third. Besides the effect of COT, we find that the scale of the atmospheric motions with which the clouds interact is also critical to their lifetime.

1. Introduction

For several decades the lifetime of shallow cumulus clouds has been a topic of theoretical, numerical, and observational studies (Chen et al., 2022; Eytan et al., 2022; Heus & Seifert, 2013; Jiang et al., 2006; LeMone & Pennell, 1976; Rauber et al., 2007; Romps et al., 2021; Seelig et al., 2021). Ideal conditions for the formation of shallow marine cumulus (SMC) clouds require a moderate surface heat flux over a warm ocean surface with weak vertical wind shear and large-scale subsidence which is common to the trades (Brueck et al., 2015; Nuijens et al., 2014). SMC form below the inversion layer that separates the convective boundary layer (CBL) from the free atmosphere. They modify the distribution of temperature and moisture within the CBL (Weckwerth et al., 1996) and vent air from the CBL into the free atmosphere (Bony et al., 2017; Derbyshire et al., 2004; Zhang et al., 2003).

Together with the polar easterlies and the mid-latitude westerlies, the trades are part of the primary atmospheric circulation that acts on the planetary scale. They form the basis of secondary and tertiary atmospheric circulation patterns that act on the synoptic and the meso-to microscale, respectively. The characteristics of meso- and synoptic-scale motions are expressed in dynamic regimes with distinct timescales. These motions are turbulent while the planetary-scale circulation is irregular and not fully turbulent (Lorenz, 1984; Seelig et al., 2012). However, all dynamic regimes are connected and the kinetic energy spectrum reflects how energy is transferred between them (Nastrom et al., 1984). As clouds are a part of the turbulent field, the distribution of cloud lifetime should therefore resemble the characteristics of different dynamic regimes (Seelig et al., 2021).

Tracking clouds in satellite data depends on pattern recognition of a cloud field advected with the mean wind. Hence cloud lifetime is closely connected to the distance they move. The mean wind is associated with momentum and kinetic energy. From that point of view, the cloud lifetime connected to processes related to synoptic

scale motions is expected to follow a −3 power law (Charney, 1971). In contrast, the lifetime of clouds connected to mesoscale motions or processes related to isotropic turbulence in the inertial subrange should follow a −5/3 power law (Kolmogorov, 1941). The investigation of the lifetime of SMC based on model studies, for which all properties - especially the 3d wind field - are available, reveals an exponential or gamma-like distribution (Heus & Seifert, 2013). The analysis of SMC that were tracked in geostationary satellite observations over a subtropical northeastern Atlantic, reveals lifetime distributions that fit the theoretically expected slopes reasonably well considering the limited spatio-temporal resolution of the observations (Seelig et al., 2021). However, cloud lifetime is also coupled to the optical and microphysical properties of the clouds and how those are affected by the presence of aerosols. Enhanced concentrations of cloud condensation nuclei at constant cloud liquid water path lead to smaller droplet effective radii and to an increase in cloud albedo (cloud albedo effect; Twomey, 1974) while the resulting suppression of precipitation causes an increase in cloud liquid water path, cloud fraction, and cloud lifetime (cloud lifetime effect; Albrecht, 1989).

The increased spatial and temporal resolution of observations with the latest generation of geostationary sensors together with an upgrade to the cloud-tracking toolbox of Seelig et al. (2021) considered here allows to extend the data set of tracked SMC and the evolution of their physical properties to shorter lifetime, smaller size, and more reliable trajectories for larger clouds.

This study is based on observations with the Advanced Baseline Imager (ABI; Schmit et al., 2017) on the Geostationary Operational Environmental Satellite (GOES)-16 at 75.2 W during the ElUcidating the RolE of Cloud–Circulation Coupling in ClimAte (EUREC^{4}A; Stevens et al., 2021) field campaign between 22 January and 13 February 2020 east of Barbados. The article is organized as follows. Technical information about the used data, upgrades in the cloud-tracking toolbox, and filtering procedures are presented in Section 2. Statistics of tracked clouds and the temporal evolution of the physical properties of daytime SMC is discussed in Section 3. A summary of the results and a conclusion are provided in Section 4.

2. Data and Methodology

2.1. GOES-16 ABI and the Cloud Physical Property Data Set

During the EUREC^{4}A campaign from 22 January to 13 February 2020, the GOES-16 ABI was set to operate in its mesoscale-scan mode with a temporal resolution of 1 min and a spatial resolution of 2×2 km^2 at nadir within a $1{,}000 \times 1{,}000$ km^2 nadir field of view. The Binary Cloud Mask (BCM; Heidinger & Straka, 2013; Heidinger et al., 2020) is used for tracking clouds. Verification of the BCM over the contiguous United States reveals 90.9% probability detecting clouds and 74.8% accuracy detecting clear sky, respectively (Jiménez, 2020; Luebke et al., 2022). Pixels labeled “cloudy” and “probably cloudy” are considered to compile binary 2d images for the cloud identification algorithm (Seelig et al., 2021).

Cloud physical properties (CPPs) are retrieved from GOES-16 ABI measurements. Relative time series of CPPs for tracked clouds are compiled for (a) cloud top temperature (CTT), cloud top height (CTH), cloud top pressure (CTP) (Schmit et al., 2017), (b) cloud optical thickness (COT), cloud droplet effective radius (CDER), and cloud water path (CWP) (Walther et al., 2013; Wood & Hartmann, 2006). Slingo and Schrecker (1982) show that the radiative properties of water clouds can be parametrized by CWP and CDER. GOES-ABI's Daytime Cloud Optical and Microphysical Properties algorithm (DCOMP; Walther & Heidinger, 2012; Walther et al., 2013) is based on the Nakajima and King (1990); Nakajima and King (1992) method that retrieves COT and CDER from measurements with a visible (0.64 μm) and a near-infrared (NIR) channel. Three NIR channel options at 1.6, 2.2, and 3.9 μm correspond to Daytime Cloud Optical and Microphysical Properties algorithm (DCOMP) modes 1 to 3, respectively. As the focus of this study is on optically thin SMC, we base the investigation of CPPs on DCOMP mode 3 which should be most sensitive to small liquid water droplets (Nakajima & King, 1990). Estimates of COT and CDER are used to calculate CWP following Bennartz (2007). The cloud droplet number concentration (CDNC) is derived using COT and CDER (Quaas et al., 2020).

Satellite retrievals of COT and CDER for liquid water clouds over the mid-latitude North Atlantic (Painemal et al., 2021) and the Southern Ocean (Kang et al., 2021) show good correlation to airborne observations. The increased spatio-temporal resolution of GOES-16 ABI compared to the GOES-13 imager is found to improve the quality of the COT and CDER retrievals (Luebke et al., 2022; Painemal et al., 2021). However, a remaining high bias compared to airborne data is expected to propagate into the retrieved CWP and CDNC.

Table 1
Number of Cloud Tracks Identified in the EUREC⁴A Region From 22 January to 13 February 2020 After Filtering

Cloud filter	Tracks
EUREC⁴A—all	2,715,178
SMC with 0.45 km ≤ CTH(t) < 3.5 km, $A_c(t)$ < 15, 000 km², and clear air	
day and nighttime	1,159,092
daytime and min(COT(t)) ≥ 0.3	402,453
daytime, min(COT(t)) ≥ 0.3 and t_c > 5 min	58,674
5 < t_c(min) < 45	57,411
45 ≤ t_c(min) < 90	1,087
90 ≤ t_c(min)	176

2.2. Cloud Tracking

An upgraded version of the cloud-tracking toolbox of Seelig et al. (2021) with revised algorithms for the cloud-velocity calculation and for linking clouds between time steps is used. The cloud-link algorithm in Seelig et al. (2021) is based on distance-matching. This method estimates the position of a cloud centroid in a subsequent time step from its current position and its velocity. A match is found by minimizing the Euclidean distance between the predicted and actual positions of cloud centroids in the next time step. Matched clouds are declared to be the same and a link is assigned. If the set conditions are fulfilled by several cloud centroids, only those with the shortest distance are linked. In case of a tie the algorithm chooses the first identified match. Details on the algorithm upgrades are provided in Supporting Information S1 (Text S1).

2.3. Filtering and Analysis of Identified Cloud Tracks

A total of 2,715,178 cloud trajectories are identified in the EUREC⁴A data set (Movie S1). The lifetime t_c and cloud area A_c per time step are derived for each cloud trajectory. The knowledge of the pixel positions of a cloud along its track is used to assign cloud optical and microphysical properties from the CPP data set. While all clouds are tracked, this study is focused on SMC. Therefore, trajectories are filtered to identify well-defined trajectories (Seelig et al., 2021):

1. *Cloud location*: All pixels at all time steps have to be over water.
2. *Cloud environment*: Clouds have to form and dissolve in clear air to obtain well-defined and consistent start and end conditions for the comparison of CPPs and to exclude merging and splitting clouds.
3. *Cloud top height*: Pixel-wise CTH(t) has to be between 0.45 and 3.50 km throughout lifetime.
4. *Cloud area*: Cloud area $A_c(t)$ must not exceed 15,000 km² throughout cloud lifetime.
5. *Cloud properties*: Clouds have to occur entirely during daytime so that retrievals of COT, CDER, CWP, and CDNC are possible (Walther et al., 2013) and pixel-wise COT(t) has to exceed 0.3 for reliable CPP retrievals (Benas et al., 2017).

The number of trajectories that remain after applying the different filters is provided in Table 1. Only 58,674 out of 2,715,178 trajectories fulfill all requirements for this study. Empirical probability density functions (PDFs) of t_c and A_c are derived with equidistant logarithmic binning. To assess the effect of cloud age on the clouds properties, the data set was split further into three intervals of cloud lifetime: short (<45 min), medium (between 45 and 90 min), and long (≥90 min). The first interval covers the range of the −5/3 scaling while the other two cover the range of the −3 scaling in Figure 2.

Time series of the spatial median CPPs per time step are inferred for each trajectory. This doesn't apply to A_c as there is only one cloud area per time step. For comparison, CPPs are interpolated to a relative time axis that scales t_c from 0 (trajectory start) to 1 (trajectory end). Then, time series of median CPPs and the corresponding lower and upper quartiles are calculated for each lifetime interval.

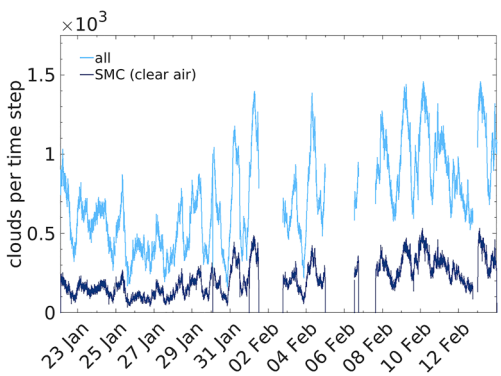

Figure 1. The number of tracked clouds per time step according to all clouds (blue) and shallow marine cumulus that passed the filtering in Table 1 (dark blue).

3. Results

3.1. Statistics of Tracked Clouds

The revised cloud-tracking toolbox is capable of tracking 98.85% of cloudy and probably cloudy pixels per time step (Figure S1 in Supporting Information S1). Figure 1 shows that the number of tracked clouds per time step varies between 150 and 1,450 with an average of 714 (not shown) during the EUREC⁴A campaign. These values depend on the larger-scale weather conditions and the diurnal cycle of boundary-layer cloud development (Brueck et al., 2015; Ruppert & Johnson, 2015; Vial et al., 2019). In general,

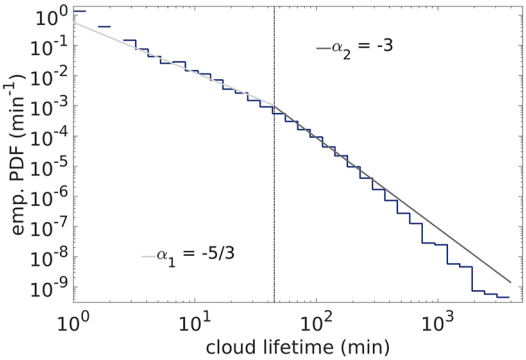

Figure 2. Empirical probability density function of cloud lifetime related to all clouds during EUREC^{4}A derived with the upgraded cloud-tracking toolbox. The light and dark gray line show the power laws expected from theory. The vertical line marks the scale break between the two regimes.

high numbers of tracked clouds are related to the presence of scattered and relatively isolated cumulus clouds. Clouds that are the target of this study, that is, SMC that form and dissolve in clear air during daytime, make up 29.8% of the total number of tracked clouds with an average of 216 clouds per time step.

Target clouds are identified with constraints on CTH. Regardless of the filters used, more than 60% of the clouds show CTHs between 0.9 and 1.4 km (Figure S2 in Supporting Information S1). These values well below 3.5 km are consistent with earlier studies of marine cumulus with median values of around 1.3 (Mieslinger et al., 2019; Seelig et al., 2021).

Figure 2 and Figure S3 in Supporting Information S1 illustrate the capability of tracking shorter-lived and smaller clouds, respectively, as a result of the high spatio-temporal resolution of observations with GOES-16 ABI. The cloud lifetime PDF (Figure 2) for all clouds during EUREC^{4}A nicely fits the −5/3 power law related to isotropic turbulence in the inertial subrange and mesoscale processes on scales of approximately 1 km to several hundreds of kilometers (Kolmogorov, 1941; Nastrom et al., 1984). The upgraded cloud-tracking toolbox is also capable covering very long-lived (large) clouds to fit the −3 power law for synoptic-scale motions. This corresponds to the enstrophy cascade from low to high wavenumber, better known as the process of geostrophic turbulence (Charney, 1971). The estimated double power law scaling parameters are −2.07 and −3.6, respectively. The scale break time that roughly separates the regimes for the meso- and synoptic-scale motions is located at 45 min and used to split the data set into short- and medium/long-lived clouds. Furthermore, reliable tracking of clouds of an area larger than 100 km^2 is an important result of the upgraded cloud-tracking toolbox (Text S2, Figures S1 and S3 in Supporting Information S1, Movie S1).

3.2. Cloud Temporal Development

This section presents the temporal evolution of the properties of the 58,674 SMC which fulfill the criteria in Table 1. For the three lifetime intervals, the median-CTT (Figure 3a) and median-CTP (Figure S4a in Supporting Information S1) curves are slightly left-skewed with a growth phase until a relative time of 0.6 followed by decay and dissolve. This is contrary to the symmetric development in Seelig et al. (2021). At formation, CTT is 289.66 ± 0.17 K for all three time intervals. However, these CTTs occur at slightly different CTPs/CTHs probably due to different data collection dates (Figures S4a, S4b in Supporting Information S1). While the short-lived clouds grow in height by merely 45 m (289.15 K, 852 hPa), the medium and long-lived clouds grow by 420 m (288 K, 828 hPa) and 625 m (287.9 K, 821 hPa), respectively. The clouds dissolve at a CTT of 289.7 ± 0.13 K, slightly above the CTP/CTH level at cloud formation. A similar left-skewed temporal evolution, in particular for medium and long-lived clouds, is found for the median cloud area A_c (Figure 3b). The occurrence of short-lived clouds is expected on small scale from a few 100 m^2 to about 10 km^2 (Koren et al., 2008). Hence, short-lived clouds are at the lower limit of ABI's spatial resolution. The interquartile A_c range for the short-lived clouds is narrow and includes clouds of an area from 4.6 up to 9.2 km^2. Clouds falling in the second and third lifetime intervals show more variability in A_c. The long-lived clouds are by far the largest with an average A_c of as much as 36 km^2 and an interquartile range from 23 to 66 km^2 that suggests mesoscale convective systems. Those clouds are likely limited in vertical growth. When they hit the inversion layer, they begin to expand horizontally, which could explain the left-skewed temporal evolution. Note, that similarities in cloud area for the three lifetime intervals at the start and the end of their lifetime results from the condition that they have to form and dissolve in cloud-free environment.

The temporal evolution of CWP (Figure S4c in Supporting Information S1) resembles that of COT in Figure 3c for all the lifetime intervals. On average, short-lived clouds reach a CWP of 60×10^{-3} kg m^{-2} while that of medium and long-lived clouds may be as high as 90×10^{-3} kg m^{-2}. The COT curves appear right-skewed with medium and long-lived clouds showing a factor of 1.5 higher COT during their lifetime compared to short-lived clouds. The increased COT during their growth phase of short-lived clouds is supported by a higher number of smaller droplets compared to the decay phase as shown in Figure S4d in Supporting Information S1 and Figure 3d.

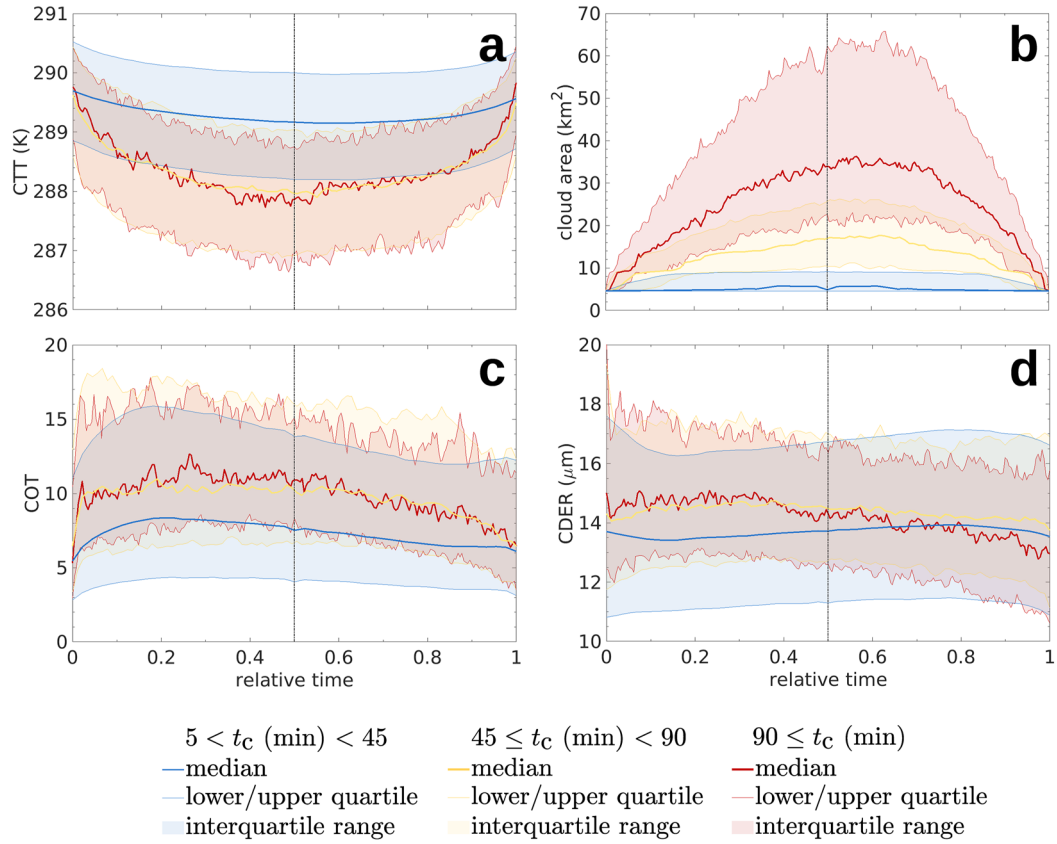

Figure 3. Temporal development of the median (bold lines) and interquartile range (shaded area) of (a) cloud top temperature, (b) A_c, (c) cloud optical thickness, and (d) cloud droplet effective radius for shallow marine cumulus with lifetimes of less than 45 min (blue), between 45 and 90 min (yellow), and longer than 90 min (red).

Medium and long-lived clouds show slightly larger droplets at lower number concentration during the growth phase compared to the short-lived clouds. After the short-lived clouds pass their maximum COT, they constantly decrease in COT as CDER increases and CDNC decreases until they dissolve (except for the last 10% of their lifetime). Their life cycle might be associated with convection, vertical transport of aerosol and/or humidity, and the formation of small droplets. The absence of convection during the decay phase and the process of collision/coalescence promote fewer but larger droplets and the cloud becomes optically thinner. Medium and long-lived clouds show increased COT and CWP during their growth. This is supported by larger droplets at similar number concentration compared to the mature and decay phases. Once the clouds have reached their largest area, they show a reduction on COT likely as a result of evaporation processes around the detrained mixed region. These processes subsequently lead to a reduction of CWP and CDER. However, small and short-lived clouds are sensitive to illumination and resolution effects. Retrievals based on the 3.9 μm channel are furthermore sensitive to the correction of emitted terrestrial and during daytime to reflected solar contribution. This might explain, for example, the initially larger CDER for the short-lived and presumably smallest clouds.

All clouds undergo processes across multiple scales, with the turbulence occurring at smaller scales while the synoptic scale modulates stability and moisture. The differences in the evolution of the medium and long-lived clouds compared to short-lived clouds are likely related to different processes connected to the dynamic regime. For example, at a smaller scale, short-lived clouds might show characteristics of a certain process A, while long-lived clouds show characteristics of another process B that is characteristic for a larger scale.

4. Summary and Conclusions

We describe the development of the properties of SMC throughout their lifetime from tracking more than 2.7 million individual clouds over the Caribbean in observations with the geostationary Advanced Baseline Imager aboard GOES-16 during EUREC^{4}A. In contrast to our earlier study of subtropical northeast Atlantic cumulus based on MSG-SEVIRI observations (Seelig et al., 2021), the improved spatio-temporal resolution of GOES-16 ABI (2×2 km^2 pixel size and 1 min) allows for also tracking clouds with a lifetime shorter than 45 min related to the dynamic regime for mesoscale motions. Improvements in the applied cloud-tracking toolbox lead to an average fraction of tracked cloudy and probably cloudy pixels of 98.85% with 150 and 1,450 clouds being tracked within the considered domain per time step. The number of tracked clouds is particularly high when broken or scattered SMC develop during typical trade-winter condition with weak to moderate subsiding motion over the warm ocean surface.

The derived PDF of cloud lifetime follows reasonably good with slopes of −2.07 and −3.6 the expected −5/3 and −3 slopes for clouds that live shorter and longer than 45 min, respectively. These slopes are related to mesoscale and synoptic scale motions and the corresponding transport of kinetic energy. Deviations to the theoretical scalings at the tails of the distribution might be due to remaining limitations in spatial resolution and the brevity of the campaign, respectively. Reliable tracking of clouds larger than 100 km^2 is achieved with the upgraded cloud-tracking toolbox. The slopes of the cloud area PDFs related to all clouds considered in this study, and Seelig et al. (2021) equals −1.75 while spanning six orders of magnitude. These values are consistent with Zhao and Di Girolamo (2007) and Wood and Field (2011). The latter authors identified a balanced contribution of small and large clouds to cloud cover when the slope of the power law distribution is sufficiently close to 2.

Our study subsequently focuses on SMC that form and dissolve in clear air during daytime as CPPs can be inferred throughout the entire life cycle of those clouds. This condition is fulfilled by on average 216 (29.8%) tracked clouds per time step of which nearly all (99%) show cloud top heights below 2.65 km. While Seelig et al. (2021) used two lifetime intervals, the EUREC^{4}A data set is grouped into three lifetime intervals. Short-lived clouds (<45 min) entirely cover the mesoscale dynamical regime, while medium (45–90 min) and long-lived clouds (≥90 min) cover the range of the synoptic-scale dynamical regime. The temporal development of most of the variables for the three time intervals show maxima at about 60% of the scaled cloud lifetime. The growth phase is found to be 20% longer than the phase of dissipation. This is different to the symmetric evolution described in Seelig et al. (2021). There are further differences to our earlier work that are related to the different sensors and changes in the tracking methodology. For instance, it is now possible to reliably track mesoscale convective systems which in turn modifies the statistics for medium and long-lived clouds.

Seelig et al. (2021) conclude that SMC of a certain area, CTH, and CDER are longer-lived for higher compared to lower COT. This work paints a more complex picture by adding that SMC clouds also live longer if they have a larger cloud area. Such clouds show similar values of median CDER and CDNC at cloud top compared to shorter-lived SMC clouds, but reveal an increase in COT and CWP of about one third. In addition to COT, the dynamic regime in which the clouds are incorporated hence also exerts an important influence on the lifetime of SMC.

Acknowledgments
We thank the Max Planck Institute for Meteorology for designing and coordinating the EUREC^{4}A campaign and the NOAA/NESDIS and University of Wisconsin-Madison/CIMSS team for providing the dedicated EUREC^{4}A GOES-16 data set. T.S., F.M., and M.T. acknowledge funding within the Franco-German Fellowship Programme on Climate, Energy, and Earth System Research (Make Our Planet Great Again—German Research Initiative, MOPGA-GRI, Grant 57429422) of the German Academic Exchange Service (DAAD), funded by the German Ministry of Education and Research. The authors thank the two anonymous reviewers for many helpful suggestions to improve the paper. Open Access funding enabled and organized by Projekt DEAL.

Data Availability Statement

A publicly available data set was analyzed in this study. The data is provided by the IPSL Compute and Data Centre at Institut Pierre-Simon Laplace and can be accessed here: https://observations.ipsl.fr/thredds/catalog/EUREC4A/SATELLITES/GOES-E/2km_01min/2020/catalog.html.

References

Albrecht, B. A. (1989). Aerosols, cloud microphysics, and fractional cloudiness. *Science*, *245*(4923), 1227–1230. https://doi.org/10.1126/science.245.4923.1227

Benas, N., Finkensieper, S., Stengel, M., van Zadelhoff, G.-J., Hanschmann, T., Hollmann, R., & Meirink, J. F. (2017). The MSG-SEVIRI-based cloud property data record CLAAS-2. *Earth System Science Data*, *9*(2), 415–434. https://doi.org/10.5194/essd-9-415-2017

Bennartz, R. (2007). Global assessment of marine boundary layer cloud droplet number concentration from satellite. *Journal of Geophysical Research*, *112*(D2), D02201. https://doi.org/10.1029/2006JD007547

Bony, S., Stevens, B., Ament, F., Bigorre, S., Chazette, P., Crewell, S., et al. (2017). EUREC^{4}A: A field campaign to elucidate the couplings between clouds, convection and circulation. *Surveys in Geophysics*, *38*(6), 1529–1568. https://doi.org/10.1007/s10712-017-9428-0

Brueck, M., Nuijens, L., & Stevens, B. (2015). On the seasonal and synoptic time-scale variability of the North Atlantic trade wind region and its low-level clouds. *Journal of the Atmospheric Sciences*, *72*(4), 1428–1446. https://doi.org/10.1175/JAS-D-14-0054.1

Charney, J. G. (1971). Geostrophic turbulence. *Journal of the Atmospheric Sciences*, *28*(6), 1087–1095. https://doi.org/10.1175/1520-0469(1971)028,1087:GT.2.0.CO;2

Chen, J., Hagos, S., Feng, Z., Fast, J. D., & Xiao, H. (2022). The role of cloud-cloud interactions in the life cycle of shallow cumulus clouds. *Journal of the Atmospheric Sciences*, *80*(3), 671–686. https://doi.org/10.1175/JAS-D-22-0004.1

Derbyshire, S. H., Beau, I., Bechtold, P., Grandpeix, J.-Y., Piriou, J.-M., Redelsperger, J.-L., & Soares, P. M. M. (2004). Sensitivity of moist convection to environmental humidity. *Quarterly Journal of the Royal Meteorological Society*, *130*(604), 3055–3079. https://doi.org/10.1256/qj.03.130

Eytan, E., Khain, A., Pinsky, M., Altaratz, O., Shpund, J., & Koren, I. (2022). Shallow cumulus properties as captured by adiabatic fraction in high-resolution LES simulations. *Journal of the Atmospheric Sciences*, *79*(2), 409–428. https://doi.org/10.1175/JAS-D-21-0201.1

Heidinger, A. K., Pavolonis, M. J., Calvert, C., Hoffman, J., Nebuda, S., Straka, W. C., et al. (2020). Chapter 6—ABI cloud products from the GOES-R series. In S. J. Goodman, T. J. Schmit, J. Daniels, & R. J. Redmon (Eds.), *The GOES-R series* (pp. 43–62). Elsevier. https://doi.org/10.1016/B978-0-12-814327-8.00006-8

Heidinger, A. K., & Straka, W. C. I. (2013). *GOES-R advanced baseline imager (ABI) algorithm theoretical basis document for cloud Mask, version 3.0*. NOAA NESDIS Center for Satellite Applications and Research. Retrieved from https://www.star.nesdis.noaa.gov/goesr/docs/ATBD/Cloud_Mask.pdf

Heus, T., & Seifert, A. (2013). Automated tracking of shallow cumulus clouds in large domain, long duration large eddy simulations. *Geoscientific Model Development*, *6*(4), 1261–1273. https://doi.org/10.5194/gmd-6-1261-2013

Jiang, H., Xue, H., Teller, A., Feingold, G., & Levin, Z. (2006). Aerosol effects on the lifetime of shallow cumulus. *Geophysical Research Letters*, *33*(14), L14806. https://doi.org/10.1029/2006GL026024

Jiménez, P. A. (2020). Assessment of the GOES-16 clear sky mask product over the contiguous USA using CALIPSO retrievals. *Remote Sensing*, *12*(10), 1630. https://doi.org/10.3390/rs12101630

Kang, L., Marchand, R. T., & Smith, W. L. (2021). Evaluation of MODIS and Himawari-8 low clouds retrievals over the southern ocean with in situ measurements from the SOCRATES campaign. *Earth and Space Science*, *8*(3), e2020EA001397. https://doi.org/10.1029/2020EA001397

Kolmogorov, A. N. (1941). The local structure of turbulence in incompressible viscous fluid for very large Reynolds numbers. *Doklady Akademii Nauk SSSR*, *30*, 301–305. Retrieved from https://ui.adsabs.harvard.edu/abs/1941DoSSR..30..301K/abstract

Koren, I., Oreopoulos, L., Feingold, G., Remer, L. A., & Altaratz, O. (2008). How small is a small cloud? *Atmospheric Chemistry and Physics*, *8*(14), 3855–3864. https://doi.org/10.5194/acp-8-3855-2008

LeMone, M. A., & Pennell, W. T. (1976). The relationship of trade wind cumulus distribution to subcloud layer fluxes and structure. *Monthly Weather Review*, *104*(5), 524–539. https://doi.org/10.1175/1520-0493(1976)104⟨0524:TROTWC⟩2.0.CO;2

Lorenz, E. N. (1984). Irregularity: A fundamental property of the atmosphere. *Tellus*, *36A*(2), 98–110. https://doi.org/10.3402/tellusa.v36i2.11473

Luebke, A. E., Ehrlich, A., Schäfer, M., Wolf, K., & Wendisch, M. (2022). An assessment of macrophysical and microphysical cloud properties driving radiative forcing of shallow trade-wind clouds. *Atmospheric Chemistry and Physics*, *22*(4), 2727–2744. https://doi.org/10.5194/acp-22-2727-2022

Mieslinger, T., Horváth, A., Buehler, S. A., & Sakradzija, M. (2019). The dependence of shallow cumulus macrophysical properties on large-scale meteorology as observed in ASTER imagery. *Journal of Geophysical Research: Atmospheres*, *124*(21), 11477–11505. https://doi.org/10.1029/2019JD030768

Nakajima, T., & King, M. D. (1990). Determination of the optical thickness and effective particle radius of clouds from reflected solar radiation measurements. Part I: Theory. *Journal of the Atmospheric Sciences*, *47*(15), 1878–1893. https://doi.org/10.1175/1520-0469(1990)047<1878:DOTOTA>2.0.CO;2

Nakajima, T., & King, M. D. (1992). Asymptotic theory for optically thick layers: Application to the discrete ordinates method. *Applied Optics*, *31*(36), 7669–7683. https://doi.org/10.1364/AO.31.007669

Nastrom, G., Gage, K., & Jasperson, W. (1984). Kinetic energy spectrum of large- and mesoscale atmospheric processes. *Nature*, *310*, 36–38. https://doi.org/10.1038/310036a0

Nuijens, L., Serikov, I., Hirsch, L., Lonitz, K., & Stevens, B. (2014). The distribution and variability of low-level cloud in the North Atlantic trades. *Quarterly Journal of the Royal Meteorological Society*, *140*(684), 2364–2374. https://doi.org/10.1002/qj.2307

Painemal, D., Spangenberg, D., Smith, W. L., Jr., Minnis, P., Cairns, B., Moore, R. H., et al. (2021). Evaluation of satellite retrievals of liquid clouds from the GOES-13 imager and MODIS over the midlatitude North Atlantic during the NAAMES campaign. *Atmospheric Measurement Techniques*, *14*(10), 6633–6646. https://doi.org/10.5194/amt-14-6633-2021

Quaas, J., Arola, A., Cairns, B., Christensen, M., Deneke, H., Ekman, A. M. L., et al. (2020). Constraining the Twomey effect from satellite observations: Issues and perspectives. *Atmospheric Chemistry and Physics*, *20*(23), 15079–15099. https://doi.org/10.5194/acp-20-15079-2020

Rauber, R. M., Stevens, B., Ochs, H. T., Knight, C., Albrecht, B. A., Blyth, A. M., et al. (2007). Rain in shallow cumulus over the ocean: The RICO campaign. *Bulletin of the American Meteorological Society*, *88*(12), 1912–1928. https://doi.org/10.1175/BAMS-88-12-1912

Romps, D. M., Öktem, R., Endo, S., & Vogelmann, A. M. (2021). On the life cycle of a shallow cumulus cloud: Is it a bubble or plume, active or forced? *Journal of the Atmospheric Sciences*, *78*(9), 2823–2833. https://doi.org/10.1175/JAS-D-20-0361.1

Ruppert, J. H., & Johnson, R. H. (2015). Diurnally modulated cumulus moistening in the preonset stage of the Madden–Julian Oscillation during DYNAMO. *Journal of the Atmospheric Sciences*, *72*(4), 1622–1647. https://doi.org/10.1175/JAS-D-14-0218.1

Schmit, T. J., Griffith, P., Gunshor, M. M., Daniels, J. M., Goodman, S. J., & Lebair, W. J. (2017). A closer look at the ABI on the GOES-R Series. *Bulletin of the American Meteorological Society*, *98*(4), 681–698. https://doi.org/10.1175/BAMS-D-15-00230.1

Seelig, T., Deneke, H., Quaas, J., & Tesche, M. (2021). Life cycle of shallow marine cumulus clouds from geostationary satellite observations. *Journal of Geophysical Research: Atmospheres*, *126*(22), e2021JD035577. https://doi.org/10.1029/2021JD035577

Seelig, T., Harlander, U., Faulwetter, R., & Egbers, C. (2012). Irregularity and singular vector growth of the differentially heated rotating annulus flow. *Theoretical and Computational Fluid Dynamics*, *27*(3), 415–432. https://doi.org/10.1007/s00162-011-0255-5

Slingo, A., & Schrecker, H. M. (1982). On the shortwave radiative properties of stratiform water clouds. *Quarterly Journal of the Royal Meteorological Society*, *108*(456), 407–426. https://doi.org/10.1002/qj.49710845607

Stevens, B., Bony, S., Farrell, D., Ament, F., Blyth, A., Fairall, C., et al. (2021). EUREC^{4}A. *Earth System Science Data*, *13*(8), 4067–4119. https://doi.org/10.5194/essd-13-4067-2021

Twomey, S. (1974). Pollution and the planetary albedo. *Atmospheric Environment*, *8*(12), 1251–1256. https://doi.org/10.1016/0004-6981(74)90004-3

Vial, J., Vogel, R., Bony, S., Stevens, B., Winker, D. M., Cai, X., et al. (2019). A new look at the daily cycle of trade wind cumuli. *Journal of Advances in Modeling Earth Systems*, *11*(10), 3148–3166. https://doi.org/10.1029/2019MS001746

Walther, A., & Heidinger, A. K. (2012). Implementation of the daytime cloud optical and microphysical properties algorithm (DCOMP) in PATMOS-x. *Journal of Applied Meteorology and Climatology*, *51*(7), 1371–1390. https://doi.org/10.1175/JAMC-D-11-0108.1

Walther, A., Straka, W., & Heidinger, A. K. (2013). *Algorithm theoretical basis document: Daytime cloud optical and microphysical properties (DCOMP), version 3.0*. NOAA NESDIS Center for Satellite Applications and Research. Retrieved from https://www.star.nesdis.noaa.gov/goesr/documents/ATBDs/Baseline/ATBD_GOES-R_Cloud_DCOMP_v3.0_Jun2013.pdf

Weckwerth, T. M., Wilson, J. W., & Wakimoto, R. M. (1996). Thermodynamic variability within the convective boundary layer due to horizontal convective rolls. *Monthly Weather Review*, *124*(5), 769–784. https://doi.org/10.1175/1520-0493(1996)124<0769:TVWTCB>2.0.CO;2

Wood, R., & Field, P. R. (2011). The distribution of cloud horizontal sizes. *Journal of Climate*, *24*(18), 4800–4816. https://doi.org/10.1175/2011JCLI4056.1

Wood, R., & Hartmann, D. L. (2006). Spatial variability of liquid water path in marine low cloud: The importance of mesoscale cellular convection. *Journal of Climate*, *19*(9), 1748–1764. https://doi.org/10.1175/JCLI3702.1

Zhang, C., Mapes, B. E., & Soden, B. J. (2003). Bimodality in tropical water vapour. *Quarterly Journal of the Royal Meteorological Society*, *129*(594), 2847–2866. https://doi.org/10.1256/qj.02.166

Zhao, G., & Di Girolamo, L. (2007). Statistics on the macrophysical properties of trade wind cumuli over the tropical Western Atlantic. *Journal of Geophysical Research*, *112*(D10), D10204. https://doi.org/10.1029/2006JD007371

References From the Supporting Information

Coopman, Q., Hoose, C., & Stengel, M. (2019). Detection of mixed-phase convective clouds by a binary phase information from the passive geostationary instrument SEVIRI. *Journal of Geophysical Research: Atmospheres*, *124*(9), 5045–5057. https://doi.org/10.1029/2018JD029772

Genkova, I., Seiz, G., Zuidema, P., Zhao, G., & Girolamo, L. D. (2007). Cloud top height comparisons from ASTER, MISR, and MODIS for trade wind cumuli. *Remote Sensing of Environment*, *107*(1–2), 211–222. (Multi-angle Imaging SpectroRadiometer (MISR) Special Issue). https://doi.org/10.1016/j.rse.2006.07.021

Lakshmanan, V., & Smith, T. (2010). An objective method of evaluating and devising storm-tracking algorithms. *Weather and Forecasting*, *25*(2), 701–709. https://doi.org/10.1175/2009WAF2222330.1

Schröder, M., König, M., & Schmetz, J. (2009). Deep convection observed by the Spinning Enhanced Visible and Infrared Imager on board Meteosat 8: Spatial distribution and temporal evolution over Africa in summer and winter 2006. *Journal of Geophysical Research*, *114*(D5), D05109. https://doi.org/10.1029/2008JD010653